Title: Some applications of PHOENICS in the underwater environment at the Defence Science and Technology Laboratory (Dstl).

Author: Dr R P Hornby, Defence Science and Technology Laboratory (Dstl), Building A32-A33, Winfrith Technology Centre, Winfrith Newburgh, Dorset, DT2 8WX

Tel: +44 (0) 1305 256014; Fax: +44 (0) 01305 256080

Email: rphornby@dstl.gov.uk

Date: November 2006

ABSTRACT

Predicting the underwater environment is a challenging problem yet is vital in assessing the performance of underwater sensors and the feasibility of maritime operations. While the Shelf Sea and Ocean models that are routinely run at the UK Metrological Office provide environmental information at relatively large scale, these models are not currently able economically to resolve the smaller scale processes such as internal wave motions that lead to a significant perturbation of the water column density structure, relatively large current pulses and enhanced turbulence and mixing. These models also employ a hydrostatic approximation that limits their application to situations where the vertical velocities are relatively small; this precludes any analysis (for example) of large amplitude internal wave propagation.

At Dstl, PHOENICS has been applied as a general purpose fluid flow package solving the full equations of motion to investigate these relatively small scale, but important, environmental effects as well as other effects relating to submersible motion. Two cases from this application set describing use of PHOENICS to predict large amplitude internal wave motions are presented in this paper.

EQUATIONS SOLVED

All case studies are solved numerically using the PHOENICS Computational Fluid Dynamics (CFD) code which solves the non-linear equations for conservation of mass, momentum, energy, turbulent kinetic energy, turbulent energy dissipation rate and tracer concentration on a fine grid. These equations (using the standard PHOENICS notation) are,

$$\frac{\partial(rf)}{\partial t} + div(ruf) = div(\Gamma_f \nabla f) + S_f$$

where f is 1 for mass conservation, u, v or w for momentum conservation, h for energy conservation, k for turbulent kinetic energy, e for turbulent energy dissipation rate and c for tracer concentration. These equations are solved for generalised stratification and arbitrary bathymetry in 2-D Cartesian coordinates with the x coordinate taken as range and the y coordinate as vertical distance. A 2-D representation is considered satisfactory as the radius of curvature of the wavefronts is large in comparison to the range distance over which significant shoaling effects take place. The KOREN high order upwind scheme [1] is used for the spatial discretisation. A standard k, e turbulence model [2] with account taken of stratification effects

is used when turbulence is to be modelled. The constant C_{3e} in the e equation is then set equal to 0.2 as recommended for stable stratification [3]. Bathymetry is modelled using cell porosity.

The bottom surface stress (first study case only) is included as a source (S_1) for the horizontal momentum equation with a value calculated using the flow velocity u_1 at 1m from the sea bottom and a drag coefficient C_D of 0.0025 [4]. The values k_{sb}, e_{sb} at the grid node distance y_{sb} from the sea bottom are calculated from expressions assuming equality of production and dissipation of turbulence (the equilibrium assumption, [5]), giving

$$S_1 = -C_D r u_1 |u_1| \quad , \quad k_{sb} = \frac{1}{0.3}\frac{|S_1|}{r} \quad , \quad e_{sb} = \frac{(\frac{|S_1|}{r})^{\frac{3}{2}}}{0.4 y_{sb}}$$

Field values of k, e , when turbulence is modeled, are initialised at t=0 to 10^{-6} (m^2/s^2) and 10^{-9} (m^2/s^3) respectively. Initial waveforms are prescribed in the domain from mathematical approximations or measured values. The ocean surface is represented as a rigid free slip lid to good approximation since the surface elevations induced by internal waves are small compared to the internal wave amplitude. The lateral boundaries can be either inflow or outlow (fixed ambient hydrostatic pressure) for the first case or cyclic for the second case.

CASE STUDIES

1. Large amplitude, shoaling internal waves in the South China Sea

Large amplitude internal waves are a common feature of the World's oceans and are frequently observed near regions of rapidly varying topography where tidal forces distort stable ocean stratification. Internal waves are important because they cause distortion of acoustic propagation paths, and produce localised current pulses which can affect drilling operations, submersible stability and water clarity due to sediment resuspension.

Recent measurements taken as part of the Office of Naval Research (ONR) sponsored Asian Seas International Acoustics Experiment (ASIAEX, 2001) in the South China Sea have provided detailed in situ evidence of many internal wave features previously inferred from satellite or theory. Relevant internal wave results from this experiment are reported by Orr and Mignerey [6] who show observations of internal waves of depression propagating into shallow water transformed into internal waves of elevation, a process that was expected from theory (Grimshaw [7]) and suggested by Liu [8] from satellite images.

PHOENICS has been used to simulate the propagation of large amplitude internal waves across water depths from 260m to 100m. The aim has been to assess the capability of a CFD code to reproduce the essential characteristics of the internal wave phase speed, shape and , localised currents by comparison with the observations from ASIAEX. The details of the location and ship track during the measurement programme of ASIAEX are shown in Figure 1. The background stratification is taken from Conductivity, Temperature and Depth (CTD)

profiles taken during the experiment. Figure 2 shows the resultant averaged density profile. A strong pycnocline is evident between 40 and 80 m depth.

The simulation uses a bathymetric slope of gradient 1 in 125 preceded by a flat bottom section of depth 260m. The latter section is sufficiently long to enable the initial, approximate Korteweg de Vries (KdV) internal solitary wave (which does not fully satisfy the full non-linear equations) to transform into a nearly steady solitary wave solution of the CFD model. In principle a more accurate initial condition could have been incorporated from the ASIAEX measurements themselves but these were not available at the commencement of the comparison exercise. The initial waveform and range velocity distribution are shown in Figure 3. The CFD model is then used to propagate the solitary wave across the continental slope from 260m to 100m over 20km using a range grid size of 15m, vertical grid size of 2m and time step of 1.25s. This choice of resolution has been guided by previous simulations, which have given reasonable results [9], [10].

Figure 4 shows the results of the CFD shoaling simulation of two solitary waves with initial amplitudes of nominally 70m and 100m (illustrated using the mid density contour in the wave). The simulations show the broadening of the initial wave with a decreasing forward propagating slope and the appearance of waves of elevation behind the main forwardly propagating wave. These elevation waves appear in ~190m deep water for the 100m initial wave and ~175m deep water for the 70m initial wave – the observations record this occurrence in water depths between 150m and 180m. The amplitudes of the waves of depression decrease in both cases, while the amplitudes of the elevation waves increase.

Figure 5 shows a comparison between the predicted phase speed for the 100m wave (considered the more representative of the experimental situation) and measurements made by Orr and Mignerey using specific locations (shown in colour) in the leading wave of depression and following depression waves. There is considerable scatter in the experimental measurements depending on which measurement location is chosen. The PHOENICS predicted phase speed was determined from a point corresponding to the largest amplitude of the lead soliton and so should most closely compare with the cyan measurement line. There is reasonable agreement with this measurement which is within the scatter defined by measurements using other locations.

Figure 6 compares predictions of the model at t=21250s with observations at a similar depth using an Acoustic Doppler Current Profiler (ADCP). This comparison shows reasonable agreement between the form of the wave profile (both in amplitude and width) and a similar distribution of range velocity in the leading section of the wave and the following elevation wave (which has the reverse circulation). Although the colour scale ranges for the predicted and measured range velocities differ significantly, the actual velocities measured are, in fact, reasonably close to the predicted values (Peter Mignerey, private communication). Note that the two velocity measurement peaks occurring to the left of the elevation wave are due to advancing solitons not considered in this CFD simulation.

Figure 7 shows the prediction of the turbulent dissipation rate in the 100m wave at t=21250s when it is transforming into a wave of elevation. Figure 8 suggests that the highest dissipation rates appear when significant elevation waves are formed – this is perhaps not surprising as

strong currents are associated with the transformation process. Also the dissipation rates predicted are at the high end of the varied oceanographic measurements shown in Figure 9 ([11], [12], University of Wales, Bangor private communication) and so the transformation process is expected to contribute significantly to enhanced mixing and sediment re-suspension. Figure 10 shows the shear distribution and flow velocity distribution as an elevation wave is forming and the maximum bed stress as a function of range. According to the Shields criterion [13] a bed shear stress of $2N/m^2$ is sufficient to lift fine sand particles with diameter ~ 0.1mm so there is the potential for fine sediment re-suspension. If this is the case then Figure 11 shows the effect of the wave in transporting re-suspended sediment (modelled initially as a passive scalar source between 15km and 16.5km range) up into the water column and towards the shore.

2. Dispersal effects due to passage of large amplitude internal waves off the Malin Shelf (north west coast of Scotland)

The Shelf Edge Study Acoustic Measurement Experiment (SESAME associated with the Shelf Edge Study (SES)) took place in the summer of 1995 off the north west coast of Scotland. SESAME was sponsored by the UK Ministry of Defence (MOD) of which Dstl forms part. One aspect of this exercise involved measurements of large amplitude (~50m) internal waves travelling towards the coast from the Malin Shelf at ~0.5m/s. Figure 12 shows the location of study and detail of soliton tracks derived from Synthetic Aperture Radar (SAR) imagery.

A typical lead soliton density profile and range velocity distribution obtained from one of the measurement stations S140 (where the water depth was 140m) were used for the PHOENICS simulation; these initial fields are shown in Figure 13 and were employed to investigate the effects of the passage of such waves on the dispersal of neutrally buoyant material initially located at different depths. For this particular case, turbulence was not modelled as the main interest was in the effect of advection. A similar spatial discretisation to the first case study was used but a longer time step was possible because elevation waves were not being simulated. Cyclic boundary conditions were used in the x direction to simulate repeated passage of such waves so a relatively short range section of ~2km was sufficient.

The results are shown in Figure 14 covering a time period of about one hour. The colours relate to concentration values initially set to unity at the three depths shown in the top left of the figure. The dark solid lines are isopycnals and the white solid lines are Richardson number contours indicating areas were turbulence is expected from flow instability. The results show significant transport effects both towards and away from the shore at mid-depth and near the surface and also reductions in the levels of concentration due to distortion of the initial material volume by shear in the wave. Near the bottom, there is less of an effect.

DISCUSSION

In general the results achieved are considered reasonable. However, for the first case in particular, which tracks an internal wave over a distance of 20km very large amounts of computing time are needed. Part of this is due to the requirement for very small time steps because of a first order accuracy restriction on the standard PHOENICS time discretisation. This situation can be improved by use of higher order temporal schemes as suggested in [14]. Both simulations use Cartesian grids which are attractive because they are orthogonal and computationally efficient. However, the stepped geometry representation of variable bottom

bathymetry (first case study) is not wholly satisfactory, so planned use of the PARSOL feature in PHOENICS [15] should allow a much better representation of the bathymetry and bottom stresses.

However, even with these changes computer times are still expected to be large and possible consideration needs to be given to use of an adaptive formulation which will automatically concentrate more grid nodes in regions of higher flow gradients and so refine the grid around a travelling wave while retaining a coarser grid in regions not influenced by the wave.

SUMMARY

A CFD model has been used to predict the propagation effects of large amplitude internal waves. Two case studies have been described. The first in an area west of the Luzon Strait with results compared with available data from the ONR sponsored ASIAEX and the second for a representative large amplitude internal wave on the Malin Shelf. In the first case, both observations and model indicate a transformation of wave shape from waves of depression to waves of elevation. There is encouraging agreement on the evolved shape of the predicted wave, its phase speed and the currents induced by the wave. Strong turbulence is predicted along the sea bed beneath the wave and in the elevated waves appearing behind the leading wave. These predicted values need verification and suitable measurement data sets are being sought. However, even modelling in two dimensions, a large number of grid nodes and very small time steps are needed to enable tracking of the wave over the required distance. This aspect may have to be addressed by using an adaptive code. The second case is much less severe on computer time but has again emphasised the dispersal capability of large amplitude internal waves near coastlines.

ACKNOWLEDGEMENTS

The author was funded by the UK Ministry of Defence as part of the Electronic Systems Research programme. The author would like to thank Dr Justin Small of the International Pacific Research Centre, Hawaii, USA for helpful discussions.

REFERENCES

1. Vreugdenhil C B and Koren B (Eds). Numerical methods for advection-diffusion problems. Vieweg 117-138 1993.

2. Launder, B. E. & Spalding D. B., The numerical computation of turbulent flows. C*omputer Methods in Applied Mechanics and Engineering*, **3**, pp. 269-289, 1974.

3. Rodi, W., Examples of calculation methods for flow and mixing in stratified fluids. *J. Geophys. Res.*, **92**, pp. 5305-5328, 1987.

4. Dyer, K. R., *Coastal and estuarine sediment dynamics.* John Wiley and Sons, 342 pp., 1986

5. Luyten, P. J., Deleersnijder, E., Ozer, J., & Ruddick, K. G., Presentation of a family of turbulence closure models for stratified shallow water flows and preliminary application to the Rhine outflow region. *Continental Shelf Research*, **16, 1**, pp. 101-130, 1996.

6. Orr M. H. & Mignerey P.C., Nonlinear internal waves in the South China Sea: Observation of the conversion of depression internal waves to elevation internal waves. *J. Geophys. Res.*, **108**, No C3, 3064, 2003.

7. Grimshaw R., Pelinovsky E., & Talipova T., Solitary wave transformation in a medium with sign-variable quadratic non-linearity and cubic non-linearity. *Physica D*, **132**, pp. 40-62, 1999.

8. Liu A. K., Chang Y. S., Hsu M. K. & Liang N. K., Evolution of nonlinear internal waves in the East and South China Sea. *J. Geophys. Res.*, **103**, C4, pp. 7995-8008, 1998.

9. Small R. J. & Hornby R. P., A comparison of weakly and fully non-linear models of the shoaling of a solitary internal wave. *Ocean Modelling*, **8**, pp. 395-416, 2005.

10. Hornby R. P. & Small J., An investigation of the shoaling of large amplitude internal waves using computational fluid dynamics. *Proc of the 6th International Conference on Coastal Engineering*, Eds C. A. Brebbia, D. Almorza & F. Lopez-Aguayo, WIT Press: Southampton, pp. 217-226, June 2003.

11. Okubo A., Some speculations on oceanic diffusion diagrams. RAPP. AM. VERB. CONS. INT. EXPL. MER. 167 pp 77-85 1974.

12. Moum J. N., Farmer D. M., Smyth W. D., Armi L., and Vagle S. Structure and generation of turbulence at interfaces strained by internal solitary waves propagating shoreward over the continental shelf. *J. Phys. Oceanog.*, 33, 2093-2112 2003.

13. Shields A., Anwendung der Ahnlichkeitsmechanik un der Turbulenz-forschung auf die Geschiebebewegung, Heft 26. Berlin: Preuss. Vers. Fur Wasserbauund Schiffbau. 1936.

14. Ochoa J. S., & Fueyo N., Large eddy simulation of the flow past a square cylinder. *PHOENICS Journal of Computational Fluid Dynamics and its Applications*, **17**, 2004.

15. Palacio A., Rodriguez A., Lombard E., Salinas M. & Vicente W., Application of the ASAP technique in the Geophysical and Industrial scales: a comparison with BFC. *PHOENICS Journal of Computational Fluid Dynamics and its Applications*, **17**, 2004.

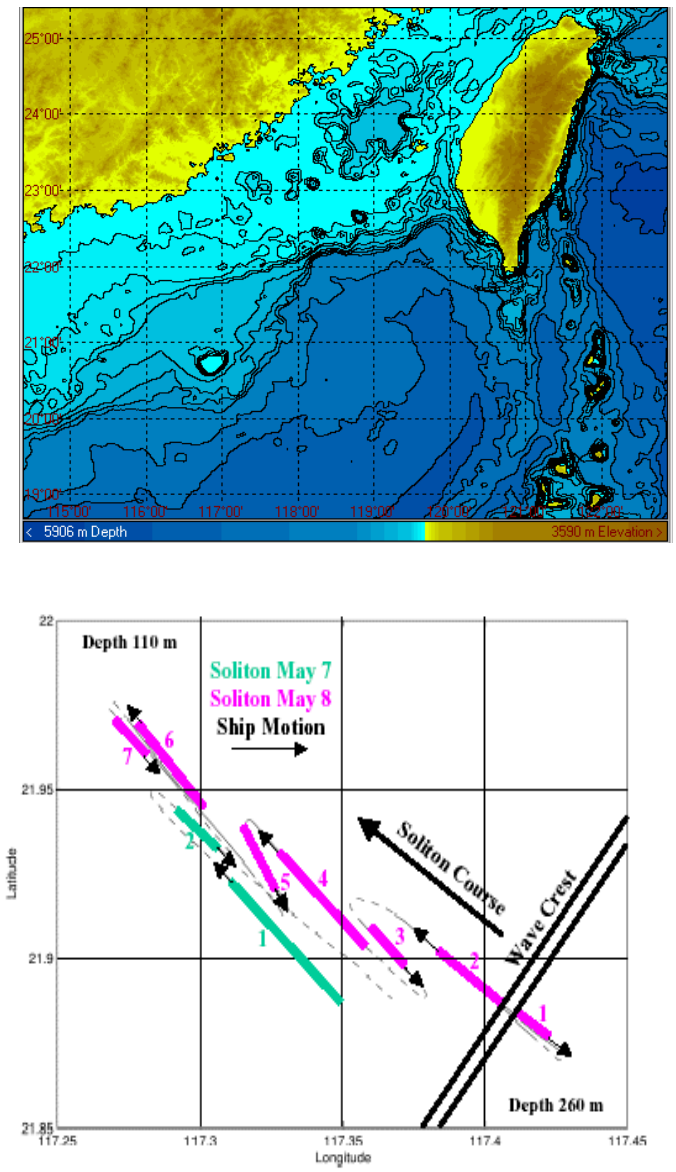

Figure 1. (Top) Bathymetry of South China Sea. (Bottom) Ship tracks crossing internal wavefronts travelling coastward on 7th and 8th May 2001 [6].

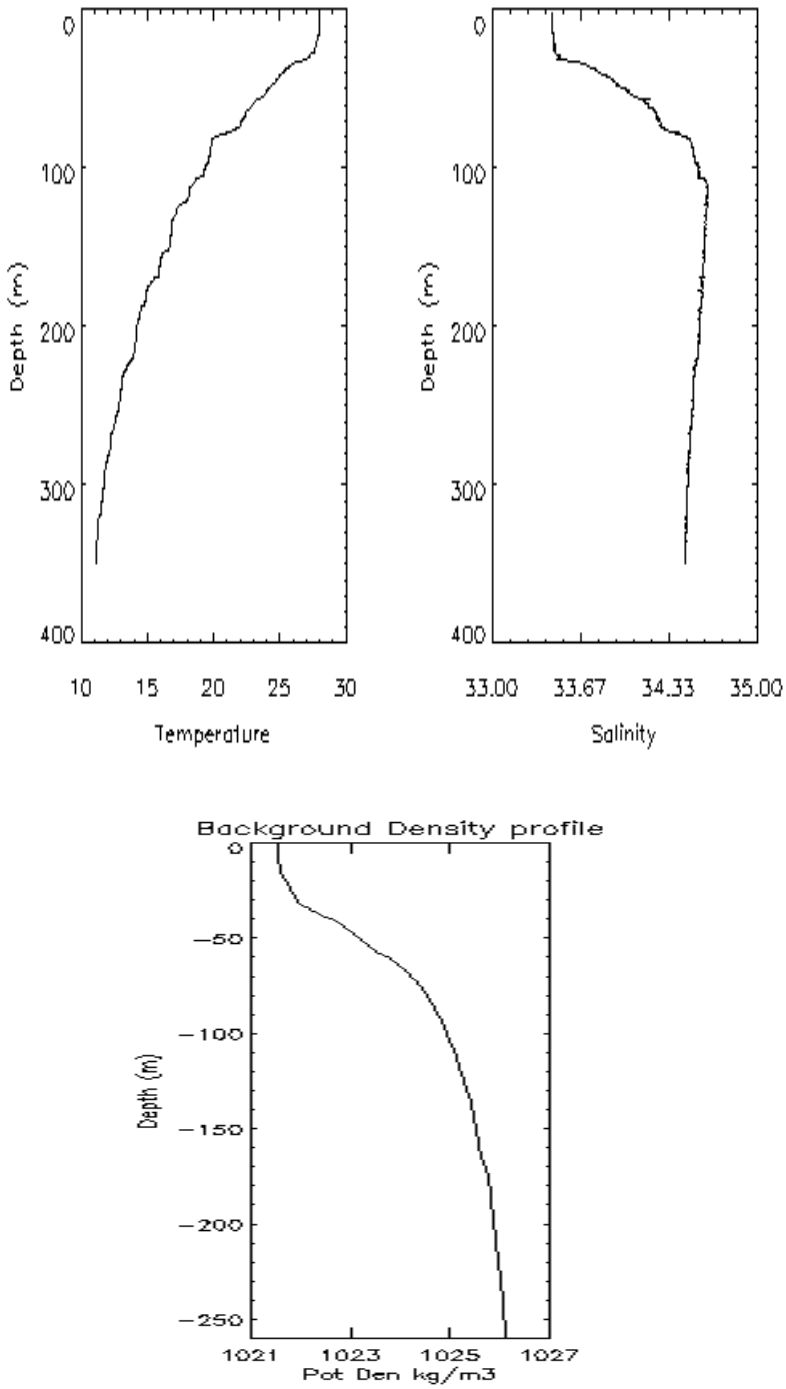

Figure 2. (Top) Typical averaged temperature and salinity profiles. (Bottom) Averaged density profile used for the PHOENICS simulation.

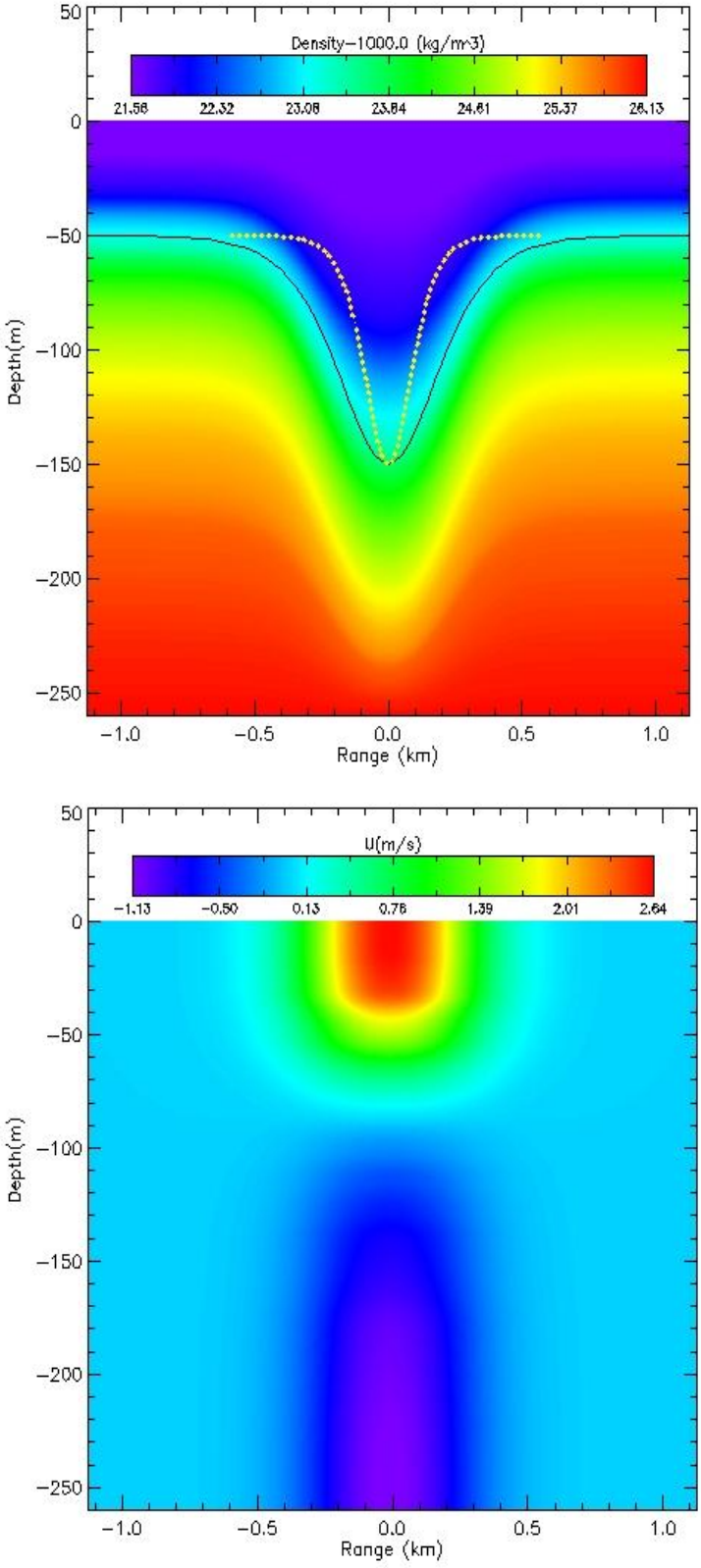

Figure 3. 100m amplitude wave case. (Top) Initial density field showing wave shape, KdV shape (dotted) and empirical KdV (solid). (Bottom) Initial range velocity field.

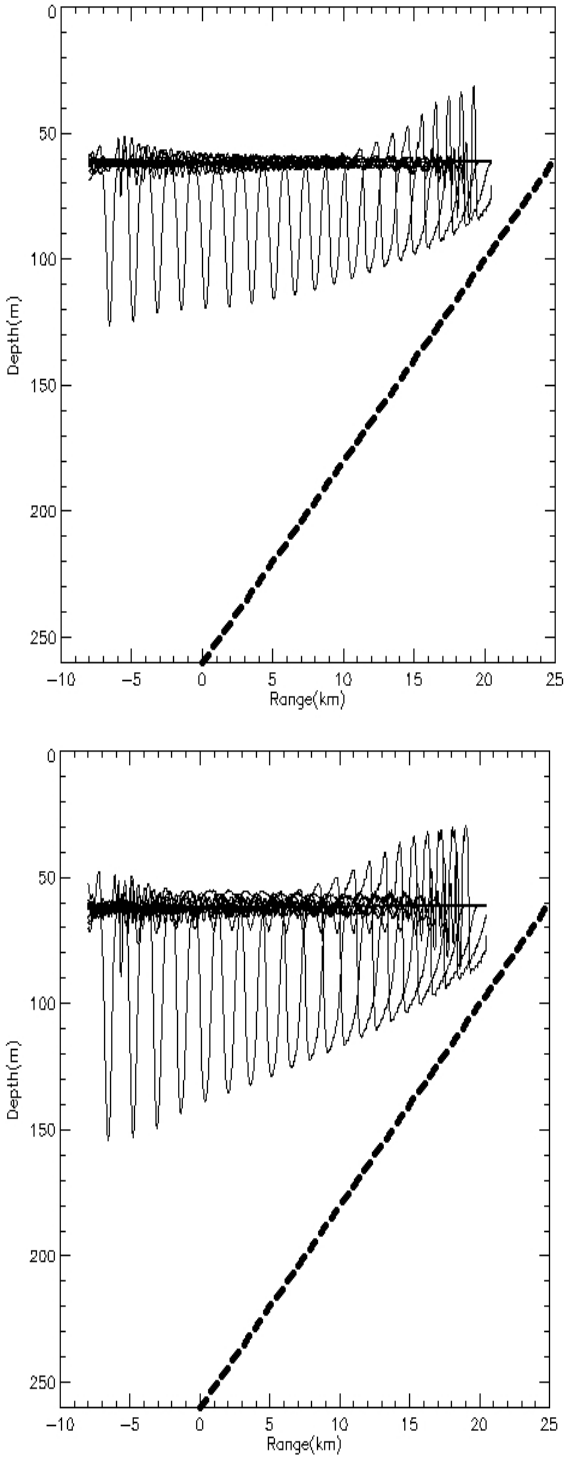

Figure 4. (Top) CFD wave evolution for initial 70m wave and (bottom) 100m wave. The time interval between each profile is 1250s. The thick dashed line represents the sea bed. Note the elevation waves appearing in 175m to 190m depth (measurements record the appearance of elevation waves between 150m to 180m depth).

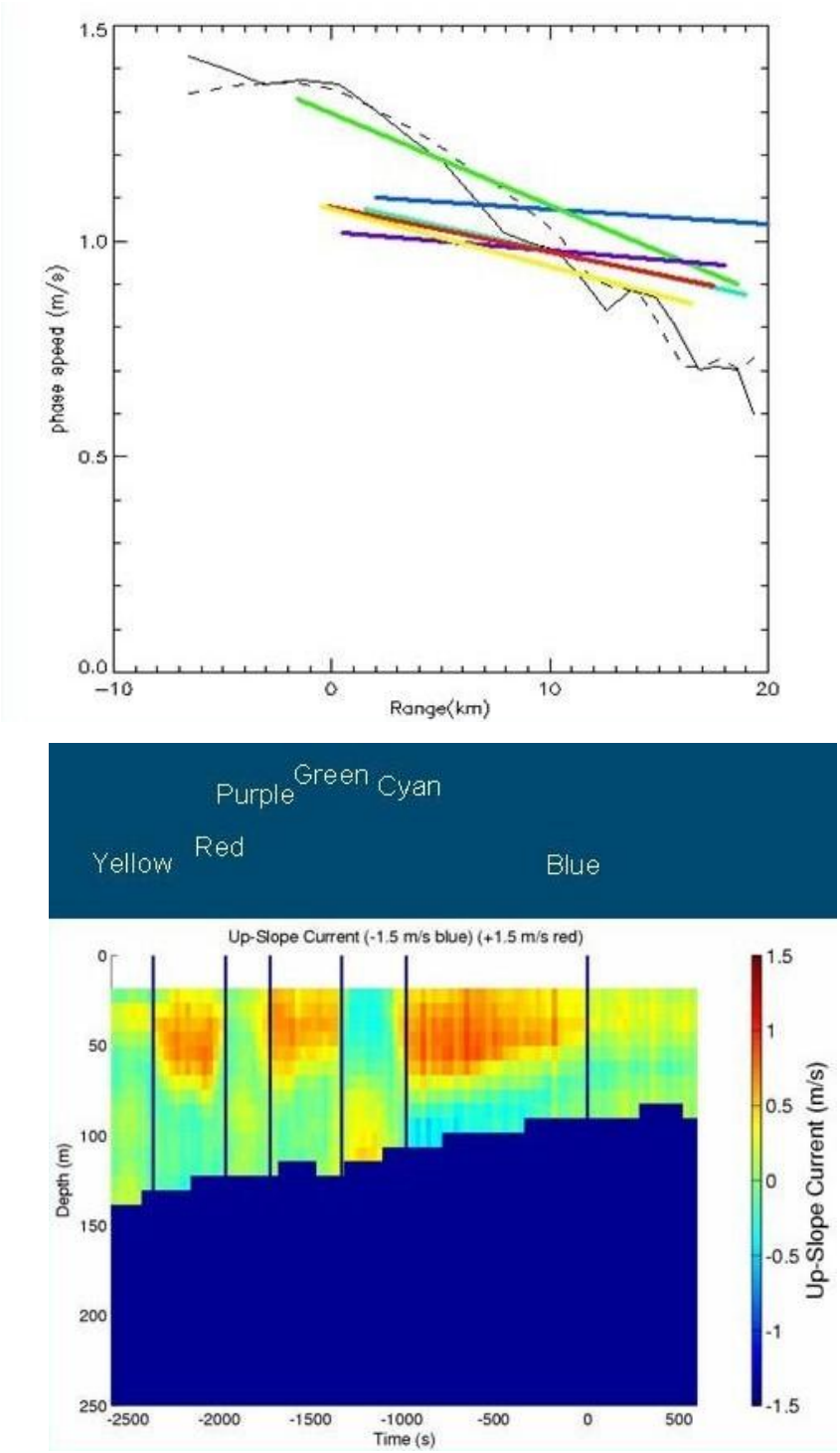

Figure 5. (Top)Variation of wave phase speed with on shelf propagation. The solid curve represents the 100m amplitude initial wave and the dashed curve the 70m amplitude initial wave. ASIAEX measurements are coloured lines (colours related to measurement positions in bottom figure), Mignerey, private communication.

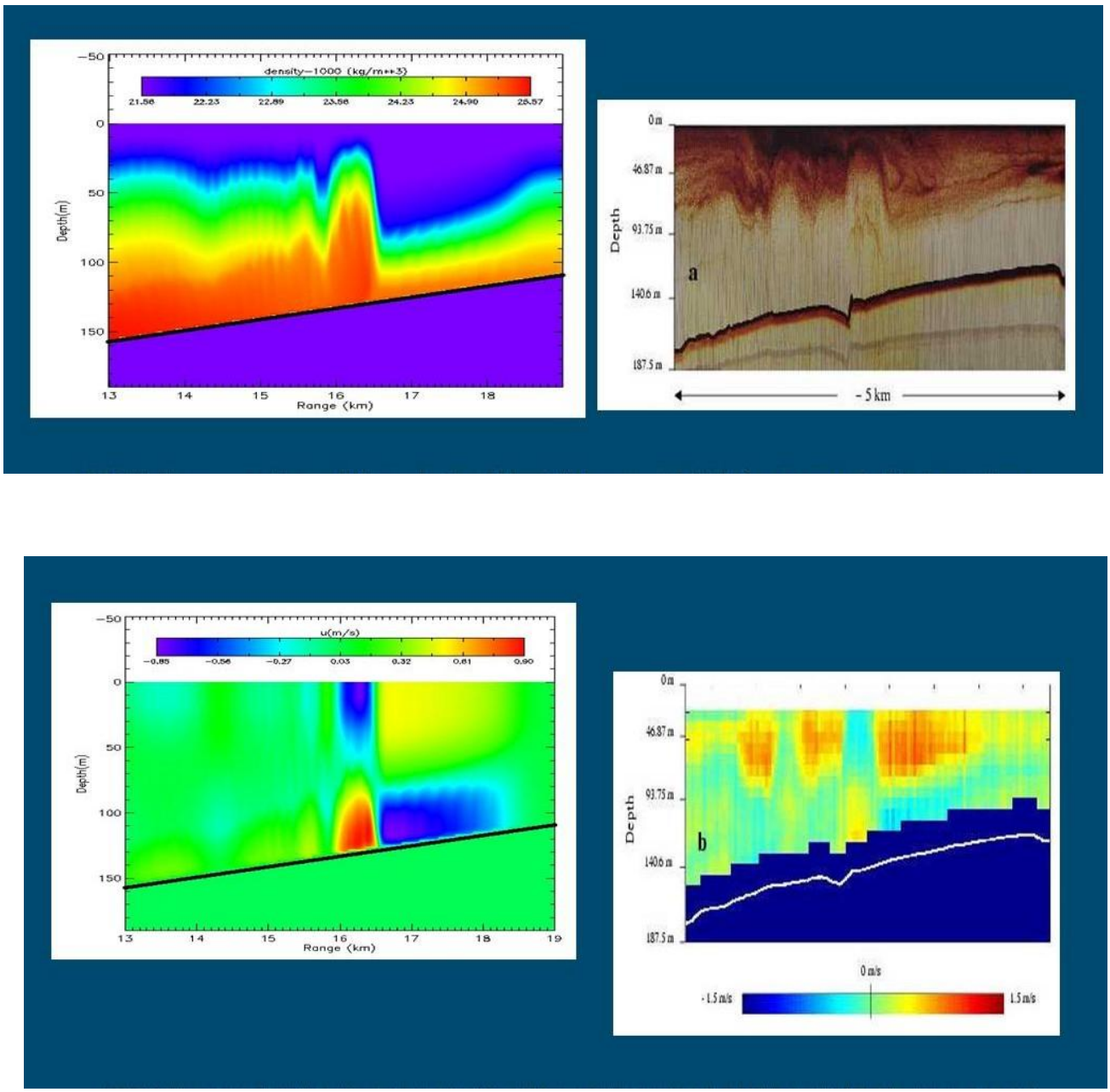

Figure 6. (Top left) PHOENICS wave profile predictions for the 100m initial wave at *t*=21250s compared with observations (top right, Orr and Mignerey, 2003) from ADCP backscatter intensity. Waves are travelling from left to right. (Bottom left) PHOENICS range velocity comparison for the 100m initial wave at *t*=21250s with ADCP (bottom right, Orr and Mignerey private communication) range velocity measurements.

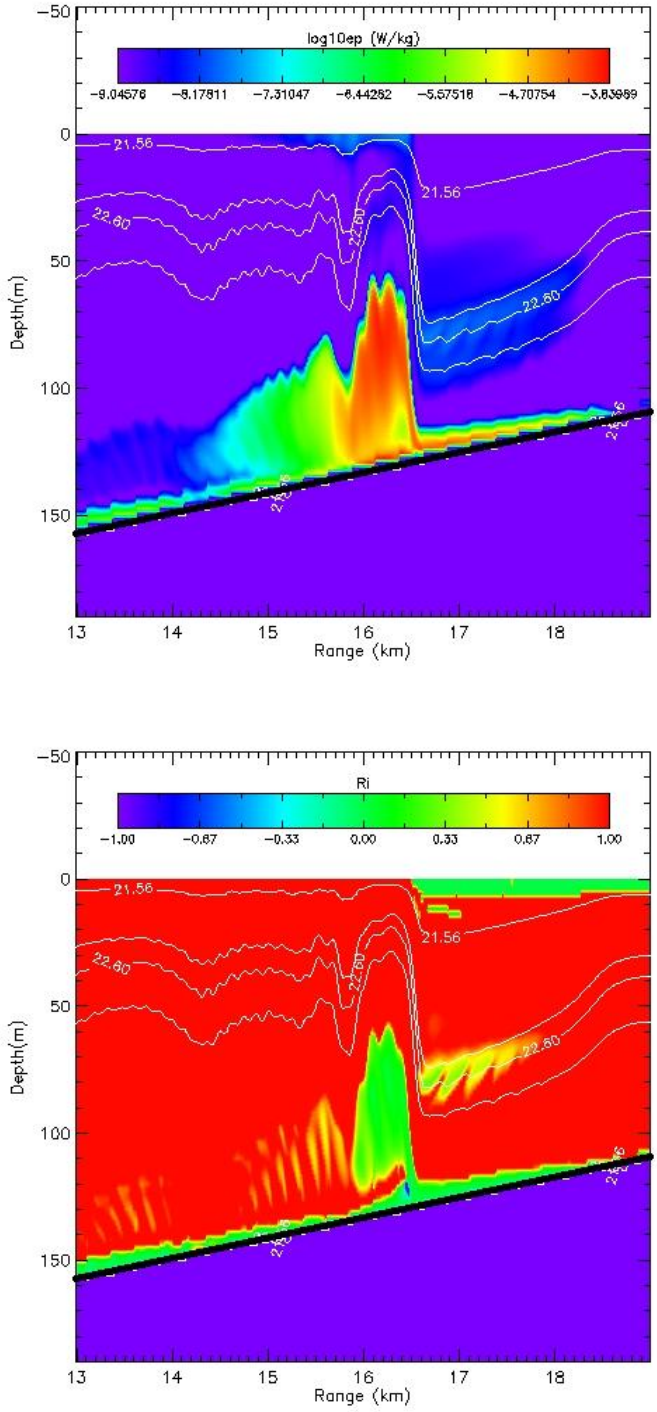

Figure 7. (Top) PHOENICS predictions of log10 of the rate of dissipation of turbulent kinetic energy per unit mass at *t*=21250s (scale range is –9.05 to –3.84). Density contours relative to 1000 kg/m^3 are superimposed to illustrate the wave shape in relation to the dissipation predictions. (Bottom) Gradient Richardson number plot.

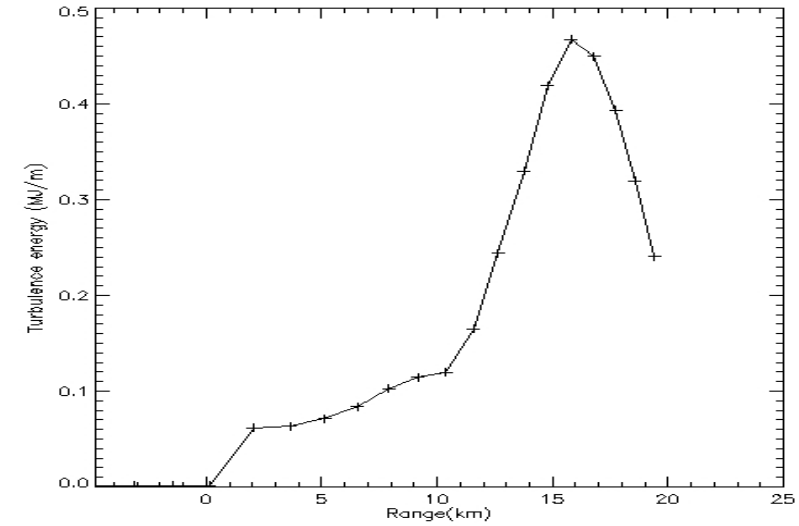

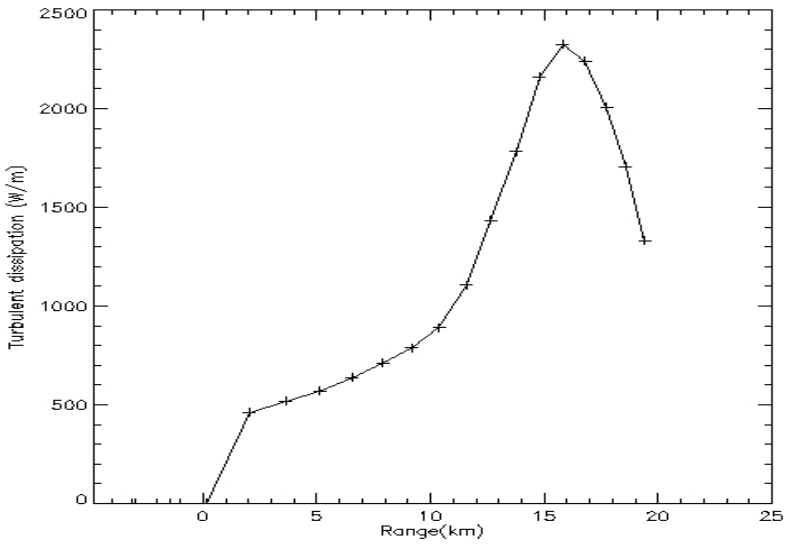

Figure 8. (Top) PHOENICS prediction of the turbulent kinetic energy integrated over a control volume 2.5km upstream and downstream of leading wave. (Bottom) PHOENICS prediction of the turbulent energy dissipation rate in a control volume 2.5km upstream and downstream of leading wave.

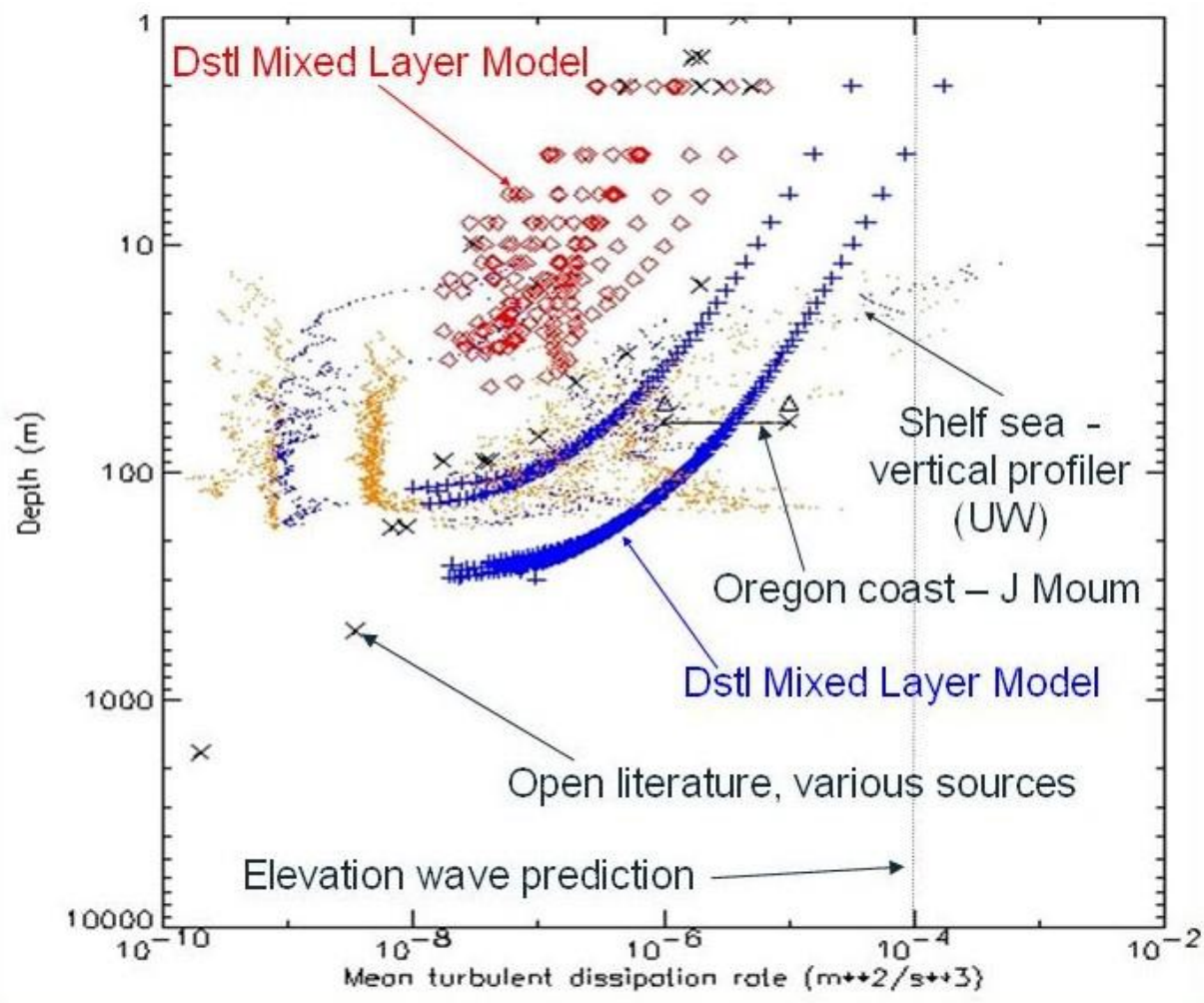

Figure 9. Turbulent dissipation rate per unit mass as a function of depth from Dstl mixed layer model , open literature sources [11], Oregon Coast [12] and measurements in European Shelf Seas (University of Wales, Bangor private communication).

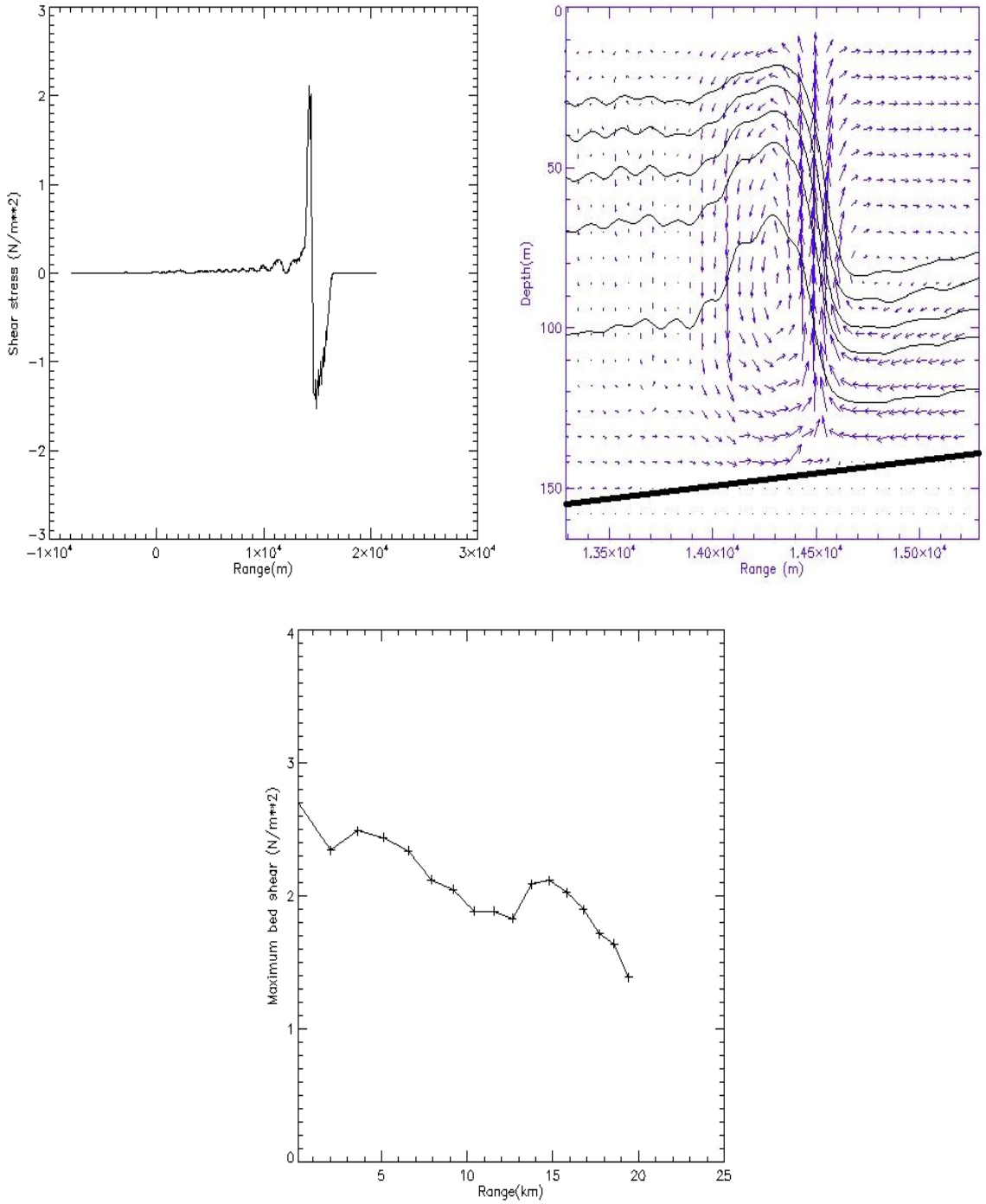

Figure 10. (Top left) Typical bed shear stress distribution prediction after formation of elevation wave (note change in sign due to flow reversal). (Top right) Corresponding flow velocity prediction. (Bottom) Maximum bed stress prediction as a function of range. A bed stress ~ 2N/m^2 would lift sand type particles with diameter < ~0.1mm (Shields criterion [13]).

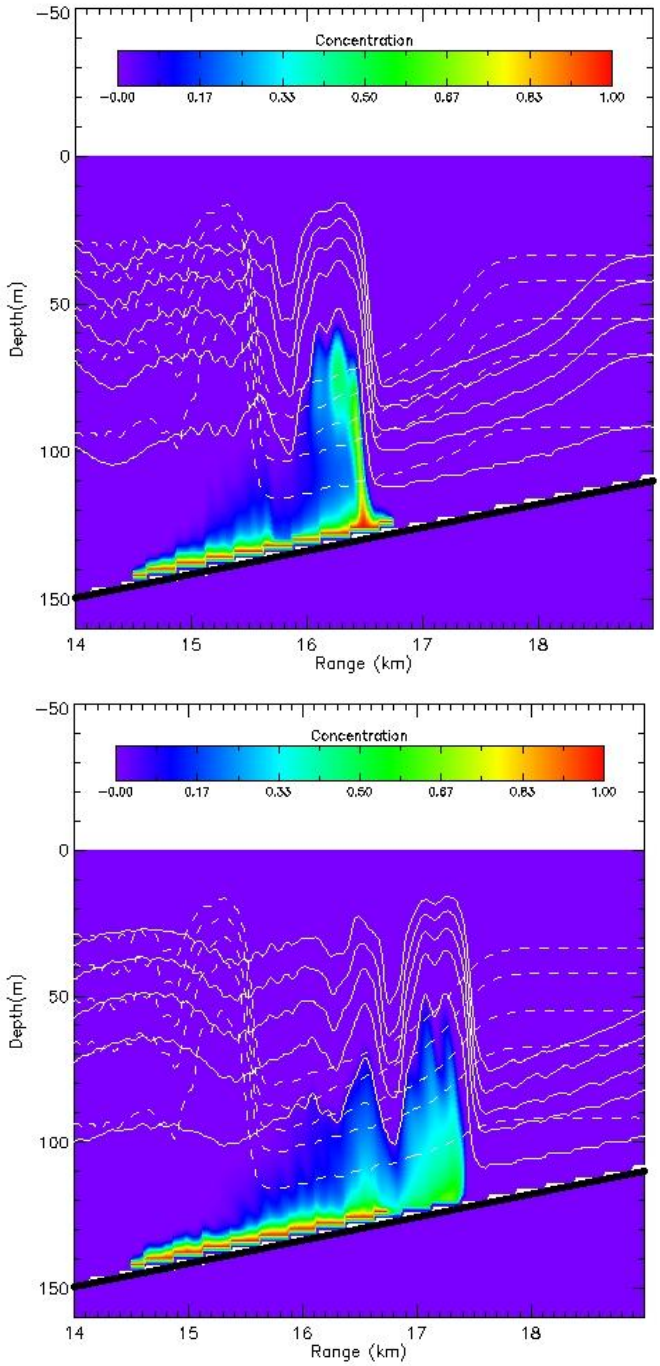

Figure 11. (Top) Predicted concentration distribution at *t*=20000s+1250s from an initial slope line source between 15km and 16.5km range. (Bottom) Concentration distribution at *t*=20000s+2500s. Wave position at t=20000s shown with dashed line. Current wave position shown as solid line.

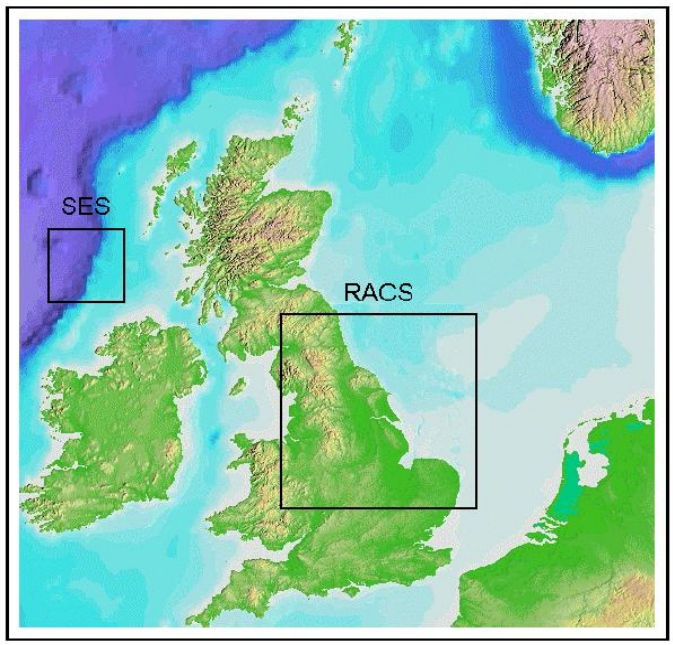

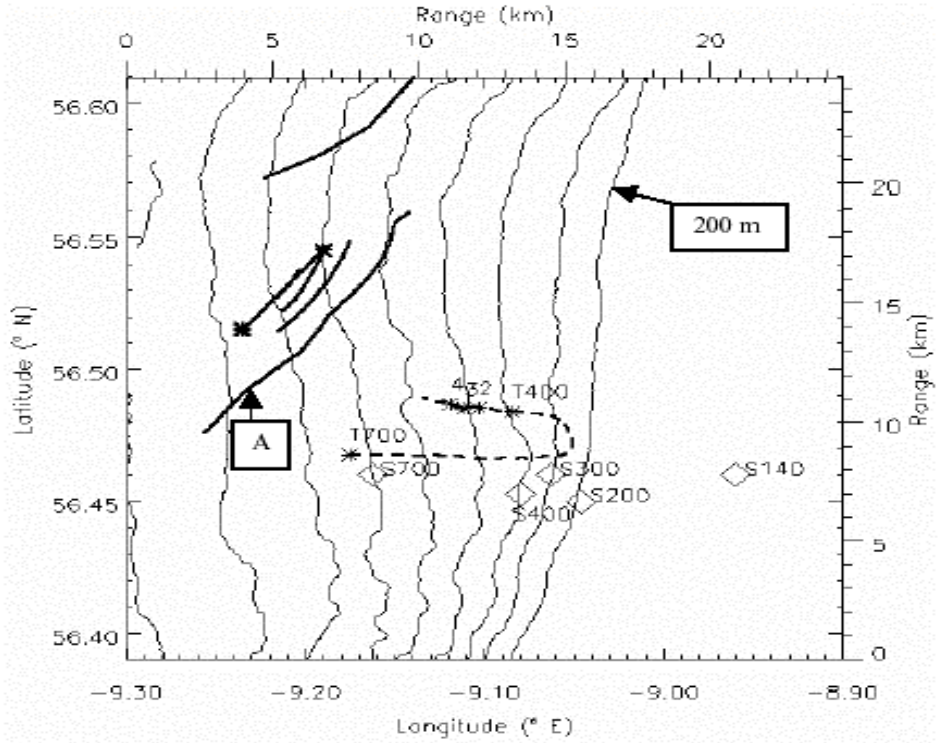

Figure 12. (Top) Shelf Edge Study (SES) area (Malin Shelf off the north west coast of Scotland). (Bottom) SES mooring marked with diamonds and labelled S700 to S140. Thermistor chain track shown as dotted line, 0000-0200 19th August 1995. 'A' marks the position of a typical lead soliton at 1136 on 20th August 1995.

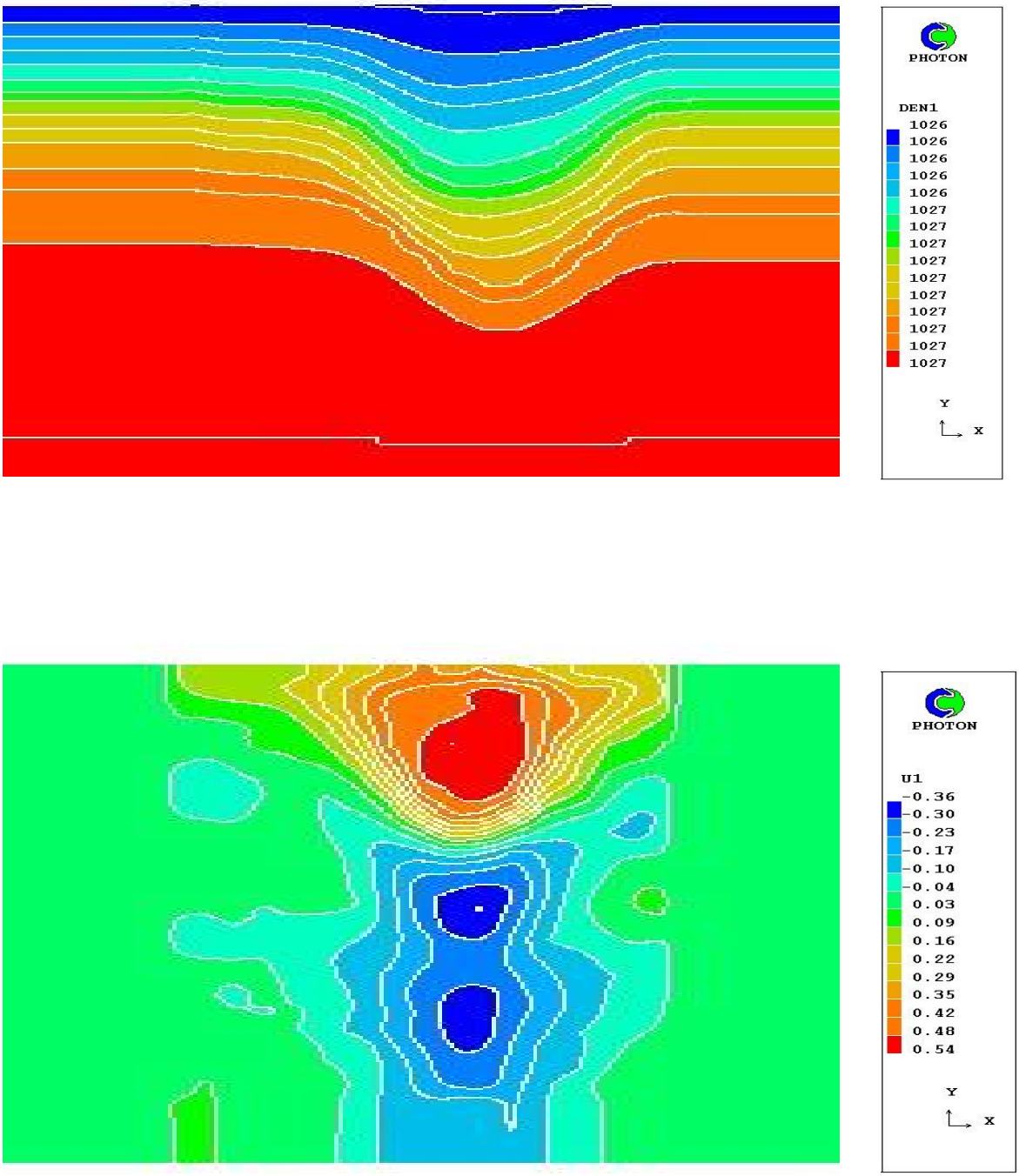

Figure 13. Malin shelf internal wave. (Top) Measured density field (kg/m^3) and (bottom) horizontal velocity field (m/s) at *t*=0s at site S140 (water depth 140m).

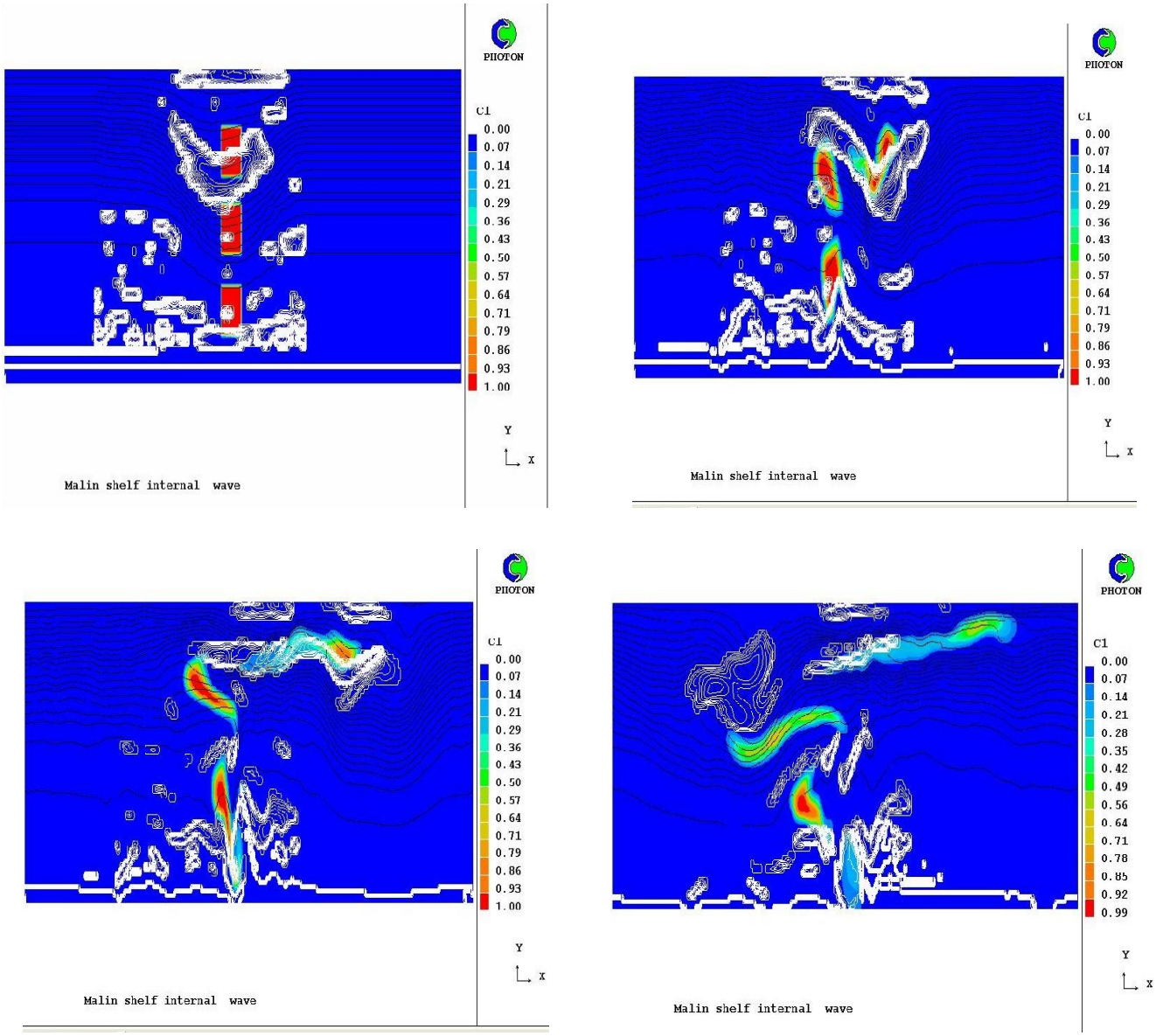

Figure 14. PHOENICS predicted effect of large amplitude internal waves of dispersing neutrally buoyant material (colour coded as concentration) initially situated at different depths. The internal wave is input to the simulation from density and current measurements made off the Malin Shelf (north west coast of Scotland). The solid dark lines shown are the wave isopycnals. The solid white lines are contours of Richardson number, indicating potential areas of turbulence. Time of simulation progresses from top left to top right to bottom left to bottom right.